JGR Space Physics

RESEARCH ARTICLE
10.1029/2021JA029678

Anomalous Reconnection Layer at Earth's Dayside Magnetopause

G. Paschmann[1], B. U. Ö. Sonnerup[2], T. Phan[3], S. A. Fuselier[4,5], S. Haaland[6,7,8], R. E. Denton[9], J. L. Burch[4], K. J. Trattner[10], B. L. Giles[11], D. J. Gershman[11,12], I. J. Cohen[13], and C. T. Russell[14]

[1]Max-Planck-Institut für extraterrestrische Physik, Garching, Germany, [2]Thayer School of Engineering, Dartmouth College, Hanover, NH, USA, [3]Space Sciences Laboratory, University of California, Berkeley, CA, USA, [4]Southwest Research Institute, San Antonio, TX, USA, [5]The University of Texas at San Antonio, San Antonio, TX, USA, [6]Birkeland Centre for Space Science, University of Bergen, Bergen, Norway, [7]The University Centre in Svalbard, Longyearbyen, Norway, [8]Max-Planck-Institut für Sonnensystemforschung, Göttingen, Germany, [9]Department of Physics and Astronomy, Dartmouth College, Hanover, NH, USA, [10]LASP, University of Colorado, Boulder, CO, USA, [11]NASA Goddard Space Flight Center, Greenbelt, MD, USA, [12]University of Maryland, College Park, MD, USA, [13]The Johns Hopkins University Applied Physics Laboratory, Laurel, MD, USA, [14]Department of Earth Planetary and Space Sciences, University of California, Los Angeles, CA, USA

Abstract Observations by the Magnetospheric Multiscale spacecraft (MMS) of an unusual layer, located between the dayside magnetosheath and the magnetosphere, alternating with encounters with the magnetosheath during an extended time period between December 31, 2015 and January 01, 2016, when the interplanetary magnetic field was strongly southward and the Earth's dipole tilt large and negative, are presented. It appears to have been magnetically connected to both magnetosphere and magnetosheath. The layer appears to be located mostly on closed field lines and was bounded by a rotational discontinuity (RD) at its magnetosheath edge and by the magnetosphere on its earthward side. A separatrix layer, with heated magnetosheath electrons streaming unidirectionally along the field lines, was present sunward of the RD. We infer that the layer was started by a dominant reconnection site well north of the spacecraft and that it may have gained additional width, from a large drop in solar wind density and ram pressure, which preceded the beginning of the event by more than an hour. Relative to the magnetosheath, in which the magnetic field was strongly southward, this unusual layer was characterized by a less southward, more dawnward magnetic field of lower magnitude. The plasma density and flow speed in the region were lower than in the magnetosheath, albeit with Alfvénic jetting occurring at the magnetosheath edge as well as at the magnetospheric edge of the layer. The closing of the magnetic field lines requires the existence of another reconnection site, located southward/tailward of MMS.

Key Points:

- Magnetopause encounter for strongly southward interplanetary magnetic field, low solar wind Alfvén Mach number, and large dipole tilt
- Persistent and broad magnetopause layer with magnetospheric O^+ and heated magnetosheath plasma
- Inferred dominant reconnection site near northern cusp, far from the Magnetospheric Multiscale spacecraft location

Correspondence to:
G. Paschmann,
goetz.paschmann@mpe.mpg.de

Citation:
Paschmann, G., Sonnerup, B. U. Ö., Phan, T., Fuselier, S. A., Haaland, S., Denton, R. E., et al. (2021). Anomalous reconnection layer at Earth's dayside magnetopause. *Journal of Geophysical Research: Space Physics*, *126*, e2021JA029678. https://doi.org/10.1029/2021JA029678

Received 15 JUN 2021
Accepted 31 AUG 2021

1. Introduction

The process of magnetic field reconnection is thought to always, or almost always, be active somewhere on the magnetopause, the boundary between the Earth's magnetic field and the compressed interplanetary field that comprises the magnetosheath. When the field in the magnetosheath is southward, the main reconnection line is usually somewhere on the dayside at low Geocentric Solar Ecliptic (GSE) latitudes, with northward- and southward-directed Alfvénic plasma exhaust jets that are fed by plasma inflow from both sides. The field lines emanating from the reconnection line separate regions of different magnetic topology and are referred to as the outer and inner separatrix. Magnetic field lines in between the outer separatrix and the current layer are connected to the ionosphere on one side and to the interplanetary magnetic field (IMF) on the other and form a wedge commonly referred to as the magnetosheath boundary layer. The field lines sunward of the outer separatrix we will refer to as the magnetosheath proper. The width of the magnetopause layer is expected to increase with increasing distance away from the reconnection line. It usually has a width of the order of 1,000 km, with a typical duration of the order of 1 min (e.g., Phan & Paschmann, 1996), although, crossings of much longer duration have very occasionally been observed.

In this paper, we report on observations by the Magnetospheric Multiscale spacecraft (MMS) of a dayside field and plasma configuration at low GSE latitudes that is strikingly different from that described above. On a pass between December 31, 2015 and January 01, 2016, during which the Earth's dipole was

tilted strongly backwards, MMS encountered a plasma layer sandwiched between the magnetosheath and the magnetosphere proper, but having field direction and other properties very different from the magnetosheath, in which the magnetic field was mainly due southward. Starting with an outbound magnetopause crossing and ending with reentry into the magnetosphere some 10 h later, hour-long encounters with this layer were observed, in between encounters of the magnetosheath proper. Judging from a significant presence of both He^{++} and O^{+} ions in the layer, it appears to be, or have been, magnetically connected to both magnetosheath and magnetosphere, respectively. An encounter with this type of a long-duration layer is, if not unique, at least extremely unusual. For ease of reference, we will refer to this layer as the Anomalous Reconnection Layer, ARL.

A portion of the overall event has already been examined in detail by Farrugia et al. (2017). These authors interpreted the event in terms of multiple crossings of the magnetopause. In their scenario, the observed hour-long layer is the magnetosphere itself. They then used the plasma and field data to infer the presence of a reconnection site near (or at) the low GSE latitude of the MMS, as expected during strongly southward IMF. In our paper, we present and discuss data from the full event. We will show that the ARL is not the magnetopause proper, but is actively formed by high-latitude reconnection during strongly southward IMF, that is, far away from MMS, this activity being modified and modulated by the changing solar wind properties during the event.

The paper is organized as follows. In Section 2, we present the relevant observations, including upstream solar wind conditions and behavior of the Auroral Electrojet (AE) index, as well as MMS 1 observations of magnetic field and ion plasma behavior during the event. In Section 3, we discuss the properties of the boundary separating the new structure from the magnetosheath proper, and also those of the magnetopause proper. In Section 4, we examine the electron and ion pitch angle distributions to infer the topology of the ARL. Finally, in Section 5, we summarize the observations and offer our own interpretation. A quantitative summary and discussion of the boundary properties, along with brief descriptions of the analysis methods are given in Appendices A and B.

2. Observations

On December 31, 2015, at about 20:15 UT, the four MMS spacecraft traversed Earth's magnetopause on their outbound orbit toward apogee and for the next 10 h observed a number of crossings into or out of the magnetosheath proper, before reentering the magnetosphere on the inbound orbit at about 06:45 UT on January 01, 2016. The plot on the left in Figure 1 shows a projection of the MMS orbit onto the GSE *xy* plane, with the two magnetopause crossings identified by red circles. The plot on the right shows the MMS orbit and the field line projections onto the GSE *xz* plane at around 08:00 UT on January 01, which is the time near the inbound magnetopause crossing. It shows a large dipole tilt in the *xz* plane of −29.7° and suggests that this reentry occurred near the outer part of the southern cusp. On the other hand, during the outbound magnetopause crossing, some 10 h earlier, the dipole tilt was small (−16°) and MMS was well away from the southern cusp, especially in latitude.

In the following, we will discuss data from the MMS 1 spacecraft: magnetic field data from the Flux-Gate Magnetometer (Russell et al., 2016); plasma data from the Fast Plasma Investigation, FPI (Pollock et al., 2016); ion composition data from the Hot Plasma Composition Analyzer, HPCA (Young et al., 2016); and energetic ion data from the Energetic Ion Spectrometer, EIS (Mauk et al., 2016), all available from the MMS Science Data Center. IMF and solar wind data are taken from the OMNI data set on NASA's CDAWeb.

2.1. Event Overview

2.1.1. Interplanetary Magnetic Field

Panels (a) and (b) of Figure 2 show that the IMF was northward/duskward before 17:00 UT on December 31, 2015. It then showed a deep magnitude dip at about 17:30 UT, followed by a more gradual rotation from northward, through duskward, to strongly southward orientation, but with a smaller sunward (positive x) component as well. The field rotation was completed at around 20:00 UT (times have been propagated to the nominal subsolar bow shock location). The mainly southward field orientation then persisted, with

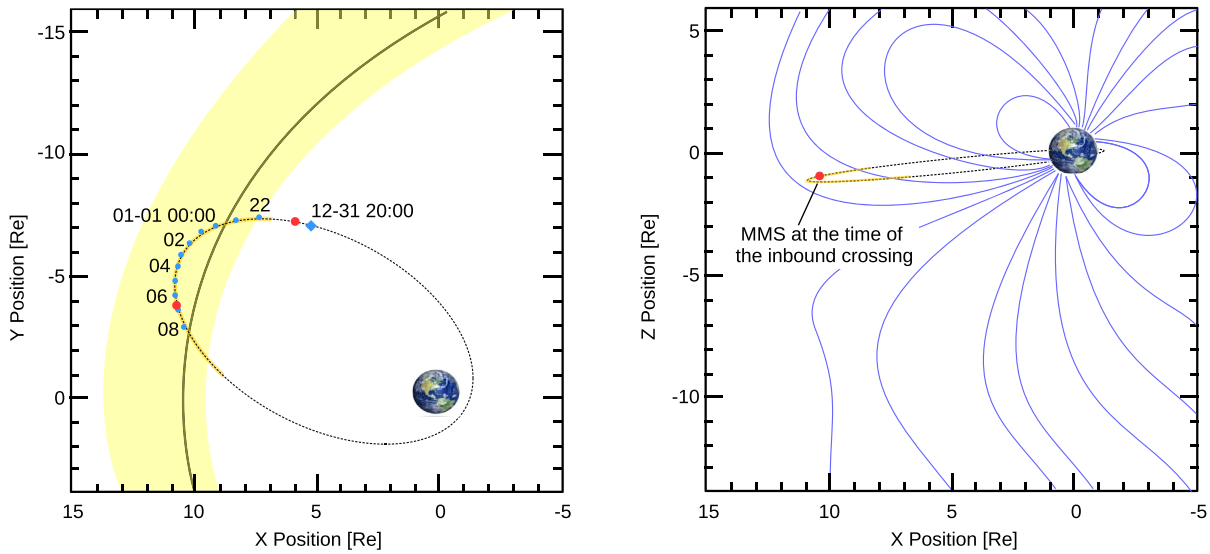

Figure 1. Left: Magnetospheric Multiscale spacecraft (MMS) orbit in the Geocentric Solar Ecliptic (x, y) plane for the times of concern, with solid red circles marking the locations of the two magnetopause crossings. Right: Orbit in the (x, z) plane, with magnetic field lines shown for the time (08:00 UT), after MMS's reentry into the magnetosphere on January 01, 2016. Note the proximity of the reentry to the southern cusp, both in latitude and longitude. During the outbound magnetopause crossing, some 10 h earlier, the southern cusp was at a longitude angle of about 12° duskward of MMS, but at much larger southern latitude (adapted from plots available at the MMS Science Data Center).

gradually dropping field magnitude, until about 05:00 UT on January 01, 2016. At that time a dawnward IMF component developed, followed by an hour of decreasing southward component to near zero at 06:45 UT, at which time the IMF recovered much of its southward direction, albeit with a remaining dawnward component. As will be discussed in Section 2.3.4, this direction then remained with little change until about 09:00 UT, after which time the IMF gradually turned increasingly northward. As argued below, the outbound magnetopause crossing and the first inbound magnetopause crossing appear to have occurred at about 20:15 UT and 06:45 UT, respectively (see panels h and i).

2.1.2. Solar Wind

Panel (c) of the figure shows that the solar wind density was high at the beginning of the plot, and with it the ram pressure (panel e), implying that the magnetopause was pushed inward, but not sufficiently far to reach the MMS location. At around 19:00 UT, the density, and with it the ram pressure, dropped abruptly, presumably causing outward motion of the magnetopause and delaying the outbound magnetopause crossing until around 20:15 UT. The density was so low that the Alfvén Mach number, shown in panel (f), became less than 2 (see also Farrugia et al., 2017).

2.1.3. Magnetospheric Activity

As expected for a long period of strongly southward IMF, there was considerable magnetospheric activity. As panel (g) of Figure 2 shows, the AE index was very low initially, but started to rise after the IMF had turned southward at around 20:00 UT, reaching ≈1,600 nT, first briefly at 22:00 UT and then for more than an hour around midnight, and going back to zero at the end of the interval shown. The hourly Dst (not shown) was −93 and −110 nT for the last hour on December 31 and the first hour on January 01, respectively.

2.1.4. Clock Angles

Panel (h) of Figure 2 shows that there were time intervals of near-equality of the IMF and the MMS1 magnetic field clock angles and intervening intervals in which the MMS clock angle was much smaller than the IMF angle. The clock angle describes the direction of the field in the GSE (y, z) plane, which for spacecraft positions not too far from local noon is approximately equal to the plane tangent to the bow shock. The coplanarity theorem requires the tangential field components upstream and downstream of the bow shock to be parallel, implying that the clock angle is conserved across it. As a consequence, the magnetosheath

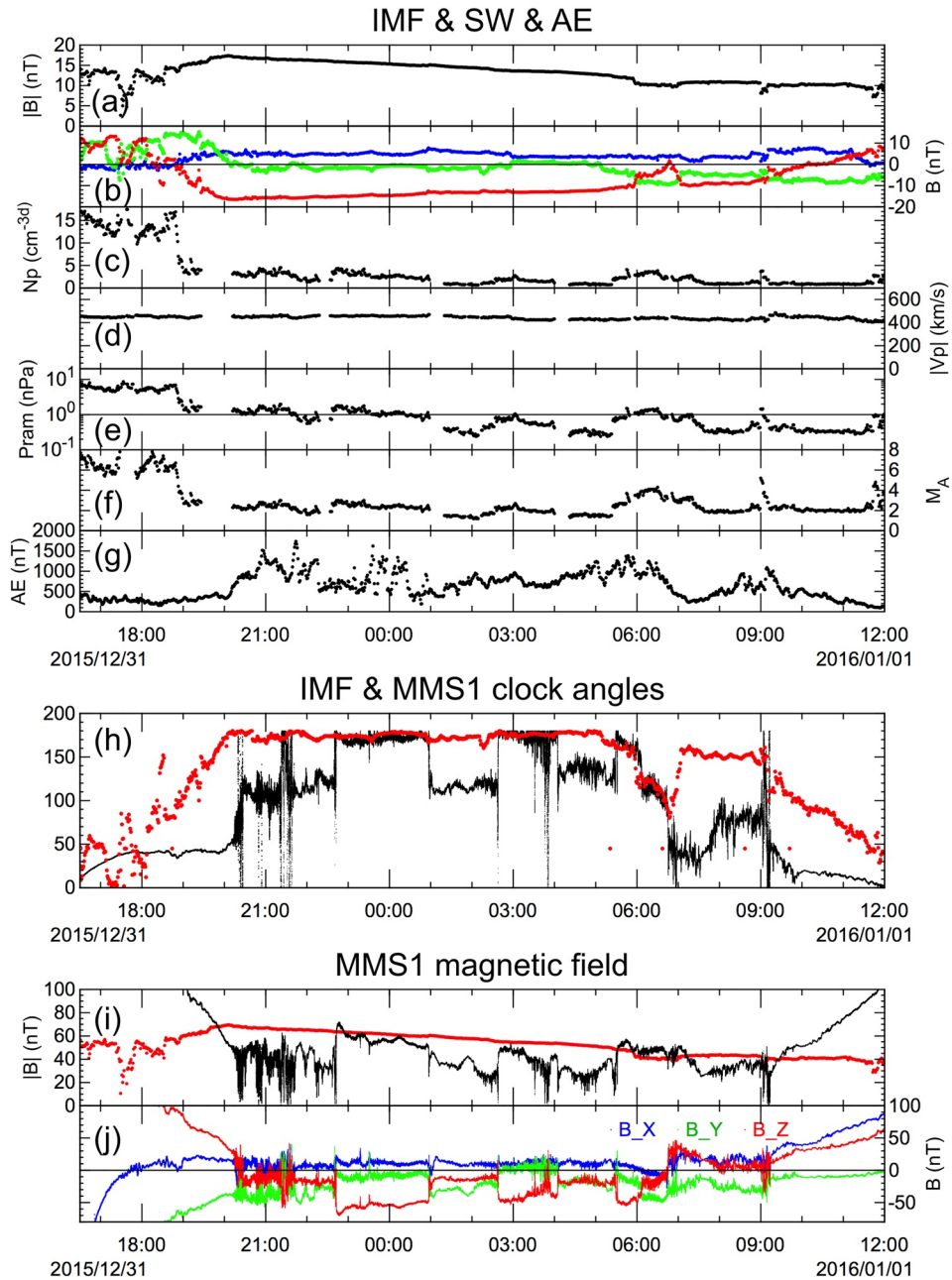

Figure 2. Overview of Magnetospheric Multiscale spacecraft (MMS) event on December 31, 2015–January 01, 2016. Panels (a) and (b) show the interplanetary magnetic field (IMF) magnitude and components (in Geocentric Solar Ecliptic [GSE], with blue, green, and red for the *x*-, *y*-, and *z*-components, respectively), followed in panels (c) and (d) by the solar wind number density and bulk speed, and in panels (e) and (f) by the ram pressure ($m_p N_p V_p^2$) and Alfvén Mach number, followed in panel (g) by the Auroral Electrojet (AE) index, all taken from the OMNI data set. Panel (h) compares the clock angles of the IMF (black) and MMS 1 (red), with 0° and 180° for fields pointing northward and southward, respectively, and with dawnward and duskward directions both shown as 90°. Panels (i) and (j) show the MMS 1 magnetic field magnitude and GSE components (from the MMS survey data). The red trace in panel (i) shows the IMF magnitude, multiplied by a factor 4 to account for field compression in the bow shock.

clock angle should be nearly the same as the IMF clock angle. For this reason, we conclude that MMS was in the magnetosheath proper in the intervals of equal clock angle, that is, near 180°, except late in the event. There were three such intervals of substantial duration plus a number of brief spikes. These magnetosheath intervals were separated by periods of substantial duration in which the MMS clock angle was around 120°,

that is, substantially less than the IMF clock angle but also not consistent with the magnetospheric clock angle of some 45°. We refer to this 120° clock angle region as the ARL. In the next section, we show that it had plasma behavior and properties significantly different from those seen in normal reconnection exhaust plumes. As discussed below, MMS entered the first inbound magnetopause crossing at 06:45 UT, when the red and black clock-angle curves in panel (g) started to diverge and then reached the magnetosphere at around 07:00.

2.1.5. MMS 1 Magnetic Field

Panel (i) of Figure 2 shows the magnetic field magnitude (black curve) and, for comparison, the IMF magnitude (red curve) multiplied by the factor 4 expected for a strong tangential shock with $\gamma = c_p/c_v = 5/3$ (e.g., Kantrowitz & Petschek, 1966). Since the shock is actually not strong during the event, the factor 4 appears to instead approximate the field compression within the magnetosheath. The plot reveals that, in the magnetosheath, the magnitude of the MMS field was dropping gradually during the event, in agreement with the gradually decreasing IMF. Together with panel (h), it also shows that the MMS field magnitude was less in the ARL than in the magnetosheath proper.

Panel (j) of the figure shows the GSE (x, y, and z) field components (blue, green, and red curves) measured by MMS. In this panel, the outbound magnetopause crossing from the magnetosphere into the ARL, is seen to start at about 20:15 UT. It is marked by a sign reversal of the B_z (red) curve and a dip of the field magnitude (black curve in panel i) to near zero. The spacecraft then entered a rapidly time variable version of the ARL in which, judging from a dip of the field magnitude to small values at around 20:50 UT, the magnetopause appears to have been briefly revisited. At about 21:30 UT, there was then a brief encounter with the magnetosheath field, after which time the field settled down to the more steady behavior typical of subsequent ARL encounters. At about 22:45 UT, MMS crossed the outer edge of the ARL and encountered the magnetosheath proper again, and then remained there until 00:56 UT on January 01.

The first inbound magnetopause crossing appears to have begun at 06:45 UT, when B_z changed from negative to positive as shown in panel (i). This time also marks where the red curve in panel (g), representing the IMF clock angle, and the black curve, representing the clock angle at MMS, start to deviate from each other, after an interval of agreement between the two, starting at 06:00 UT. In this 45-min interval, MMS was located in the magnetosheath, but the red and black curves both change a great deal. In contrast to the outbound crossing, MMS then appears to have entered almost directly into the magnetosphere, without any obvious intervening transition through the ARL (for more details, see Section 2.3.4).

Note that the magnetospheric field after 06:45 UT had an unusual orientation with B_z and B_x both positive and of comparable magnitude, and B_y also substantial but negative. This behavior is explained by the location of MMS near the southern cusp during the inbound pass, as shown on the right in Figure 1. It also appears that the spacecraft then remained close to the magnetopause for a couple of hours and that there was a brief second encounter with it shortly after 9:00 UT. After that time, MMS entered deeper into the magnetosphere proper as the field turned increasingly northward/sunward.

In summary, the magnetosheath field remained strongly southward during almost all of the events, with magnitudes that exceeded those observed immediately earthward of the magnetopause. The field in the ARL was weaker than in the magnetosheath and had a substantial negative B_y as well as a somewhat smaller negative B_z. This field direction is difficult to explain as being present in the magnetosphere itself throughout the event. It has prompted us to instead refer to the region as the ARL. The transitions from ARL to magnetosheath and vice versa are, as we will show, the result of inward/outward motion of the boundary separating the two regions. This motion appears to have been caused by variations in the solar wind ram pressure. Occasional "glitches" in the MMS clock angles, especially in the interval 03:00–04:00 (see panel g), provide evidence for momentary returns of that boundary to the MMS location.

The prior study by Farrugia et al. (2017) was focused on the subinterval 00:00–03:00 UT on 01 January, which contains two transitions between the magnetosheath proper and what they refer to as the magnetosphere. On account of its unusual magnetic field direction and other properties, we have chosen to instead identify this region as a distinct layer, the ARL, sandwiched between the magnetosheath proper and the magnetopause proper.

2.2. MMS Ion Data

Figure 3 shows the plasma ion data, together with the magnetic field data. As already mentioned, the intervals of large negative B_z are identified as magnetosheath encounters. In these intervals, the temperatures are lower than in the adjacent ARL, with the $T_\perp > T_\parallel$ anisotropy typical of the magnetosheath, and the ion densities are higher than in the ARL.

2.2.1. Ion Composition

The ion composition (panel d) is also distinctly different in the ARL, with a significant presence of O^+ ions (blue trace) and depressed but still significant presence of He^{++} (red trace), indicative of ongoing or past magnetic connection to both the magnetosphere and the magnetosheath. The O^+ population in the ARL has core energy of ≈10 keV, similar to those on closed field lines in the magnetosphere (not shown), indicating their magnetospheric origin.

2.2.2. Pressures

Panel (h) of Figure 3 shows that the total pressure (blue trace) was highly variable, presumably reflecting temporal variations in the solar wind and IMF pressures. Contrary to the usual situation, the magnetosheath pressure was dominated by the magnetic field (black trace), with $\beta \approx 0.1$ and the Alfén speed ≈ 450 km/s. By contrast, in the ARL the plasma pressure (green trace) was often larger than the magnetic pressure, with $\beta \approx 4$.

2.2.3. Ion Velocity

In the magnetosheath, the ion bulk velocity (panel e) was directed northward, with a magnitude of about 150 km/s initially, dropping to a low of about 15 km/s just before MMS reentered the magnetosphere at 06:45 UT, while in the ARL it was generally low, typically in the range 50–100 km/s, in the southward direction, but sometimes also with a duskward component. At the boundary between the magnetosheath and the ARL, the ions exhibited strong, southward directed jetting, with speeds of up to 450 km/s. Brief intervening bursts were presumably caused by momentary approaches of that boundary, caused by its back and forth motion. As will be discussed in Section 2.3, there is evidence that these velocity bursts signify the presence of a rotational discontinuity (RD) at the boundary. Velocity bursts are also seen in the inbound magnetopause layer.

2.3. Boundary Crossings

In this section, we present observations from the outbound MMS crossing from the magnetosphere into the ARL, two of the transitions between the magnetosheath and the ARL, and the inbound magnetopause crossing. Certain basic properties of the 7 boundaries identified in Figure 3 are provided in Appendix A.

2.3.1. Outbound Magnetopause Crossing Into the ARL

Figure 4 shows the outbound magnetopause crossing (starting near 20:15 UT, the time labeled t1 in Figure 3) and the subsequent first magnetosheath encounter starting at about 22:45 UT, the time labeled t2 in Figure 3. The following features are noteworthy:

1. The outbound magnetopause current layer crossing has a long duration and is highly oscillatory
2. The crossing is directly into the ARL, as evidenced by the behavior of B_z and of the ion temperature
3. As indicated by the presence of He^{++} and O^+ ions (panel d), the ARL is, or has been, connected to both magnetosphere and magnetosheath
4. There is a brief magnetosheath precursor at around 21:23 UT, as evidenced by the B_z trace in panel (a), as well as by the agreement between IMF and MMS clock angles in Figure 2
5. The $\vec{B}$ field is much noisier, and the He^{++} density somewhat higher until 21:40 UT, that is, shortly after returning to the ARL following the brief magnetosheath encounter. This transition from a highly time variable to more quiescent conditions appears to be a temporal effect rather than a spatial one caused by coexisting layers

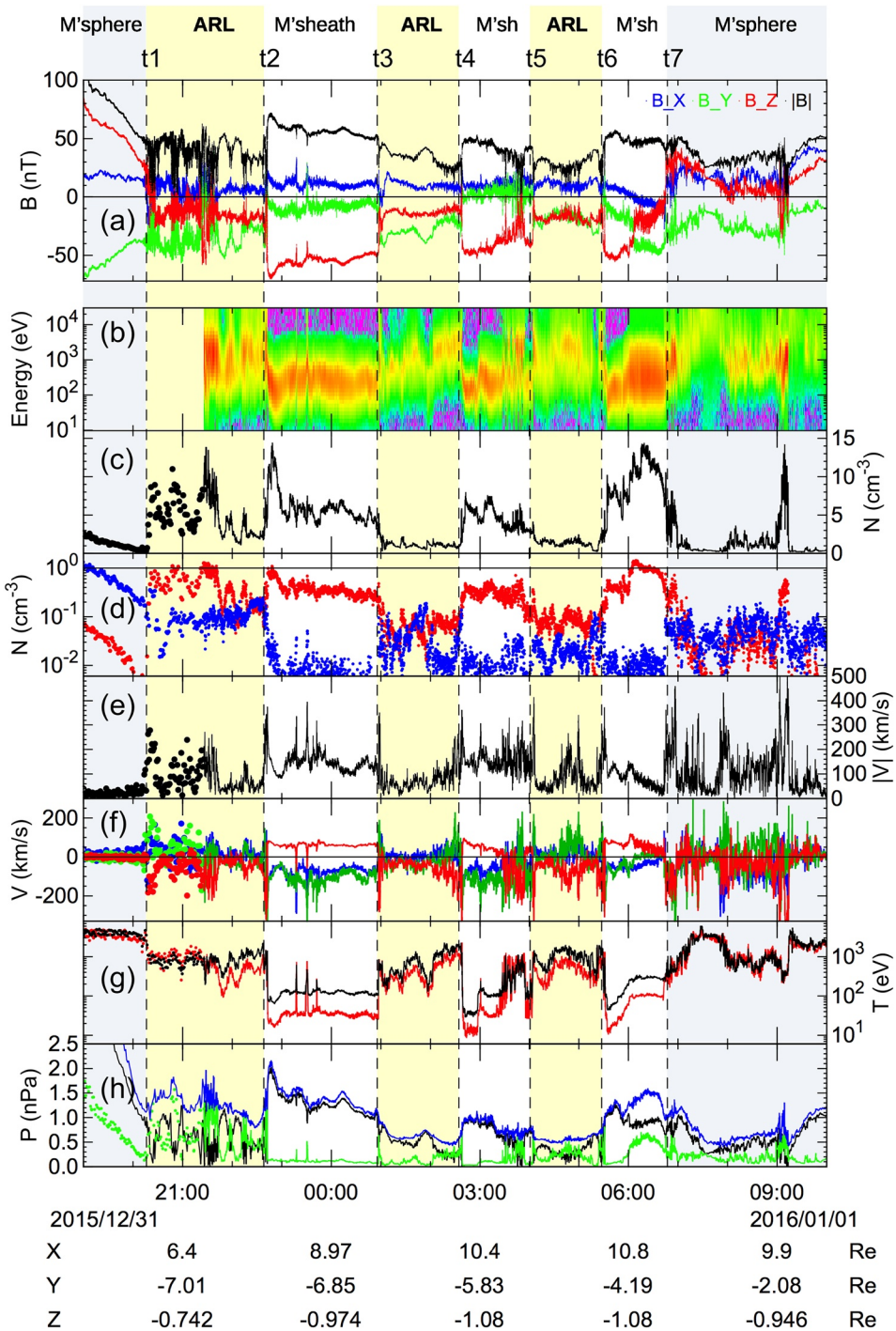

Figure 3. Overview of Magnetospheric Multiscale spacecraft (MMS) 1 magnetic field and plasma data. Panel (a): field magnitude and Geocentric Solar Ecliptic (GSE) components; panel (b): Fast Plasma Investigation (FPI) ion energy-time spectrogram; panel (c): FPI ion and Hot Plasma Composition Analyzer (HPCA) H^+ density; panel (d): HPCA O^+ (blue) and He^{++} (red) number densities; panels (e) and (f): FPI ion and HPCA H^+ bulk velocity magnitude and components; panel (g): FPI ion and HPCA H^+ temperatures ($T_\perp$ in black, $T_\parallel$ in red); panel (h): magnetic field, ion and total pressures in black, green, and blue, respectively. FPI data are from the "fast" mode, with 4-s cadence, available only after 21:20 UT on December 31. HPCA data are from the "survey" mode, with 10-s cadence; they are shown until the start of the FPI data. UT (in hh:mm) and MMS1 positions (in GSE) are given along the bottom. Dashed vertical lines labeled t1–t7 mark the boundary crossings. The Anomalous Reconnection Layer (ARL) and magnetosphere are shaded in yellow and light gray, respectively, while the magnetoshath is unshaded.

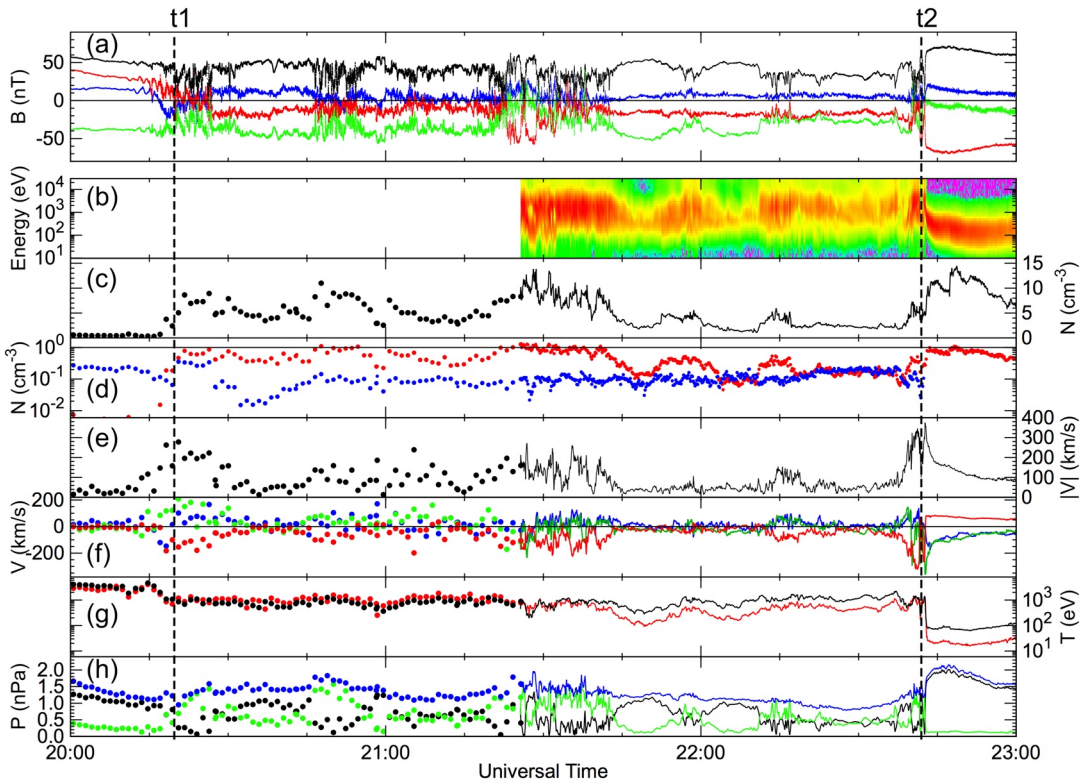

Figure 4. Outbound magnetopause crossing into the Anomalous Reconnection Layer, at the time labeled t1, and subsequent transition into the magnetosheath, at time t2. Format is the same as in Figure 3. No O^+ densities are shown in panel (d) after 22:40 UT because of "bleed over" from the high H^+ flux. Note that Fast Plasma Investigation plasma data are not available until about 21:20 UT.

6. Southward directed plasma jetting at the magnetopause crossing is observed in the HPCA proton velocities.

2.3.2. ARL-to-Magnetosheath Crossing

Starting at about 22:40 UT (labeled t2 in Figure 4), MMS crosses from the ARL into the magnetosheath. Figure 5 shows high-resolution (burst-mode) data for that crossing, which illustrate its complicated, highly nonmonotonic nature. MMS 1 was first in the ARL, then partially crossed into the magnetosheath, recognized by the large drop in B_z at 22:41:40, then made a partial return to the ARL, before fully entering the magnetosheath at 22:42:40 UT. This latter transition is recognized by a drop in temperatures, an increase in temperature anisotropy, and a rise in total ion density. As noted earlier, the field magnitude is higher in the magnetosheath than in the ARL. Ion jetting is pronounced, with velocities reaching 450 km/s. The individual velocity components are anticorrelated with the corresponding components of $\vec{\boldsymbol{B}}$ (for a discussion of the density and field peaks accompanying this crossing, see Appendix A).

The bottom frame of the figure shows the results of the Walén test (see Appendix B) for the interval 22:39–22:43 UT, in the form of a component-by-component comparison between $\vec{\boldsymbol{V}}' \equiv (\vec{\boldsymbol{V}} - \vec{\boldsymbol{V}}_{\rm HT})$, the plasma velocity in the deHoffmann-Teller (HT) frame, and the Alfvén velocity or its inverse, corrected for pressure anisotropy, such that $\vec{\boldsymbol{V}}_{\rm A} = \vec{\boldsymbol{B}}[(1-\alpha)/\mu_0\rho]^{0.5}$. The values of the anisotropy factor α are based on the perpendicular and parallel ion temperatures shown in panel (g). The good agreement of the velocities indicates that the flows, as seen in the HT frame, are indeed approximately anti-field aligned and Alfvénic. The relevant numbers are: a deHoffnann-Teller correlation coefficient (HTcc) = 0.950, a Walén correlation coefficient (Wcc) = −0.904, and a Walén slope (Wsl) = −0.729 (see Appendix B). They suggest that MMS encountered an RD, with the negative sign indicating that the flow in the HT frame was antiparallel to the magnetic field throughout the boundary. In spite of similar plasma densities on the two sides, there is no evidence of inflow into the boundary from both sides. The flow appears to have been consistently antiparallel to the field, which implies plasma transport across the RD, from the magnetosheath into the ARL. Such

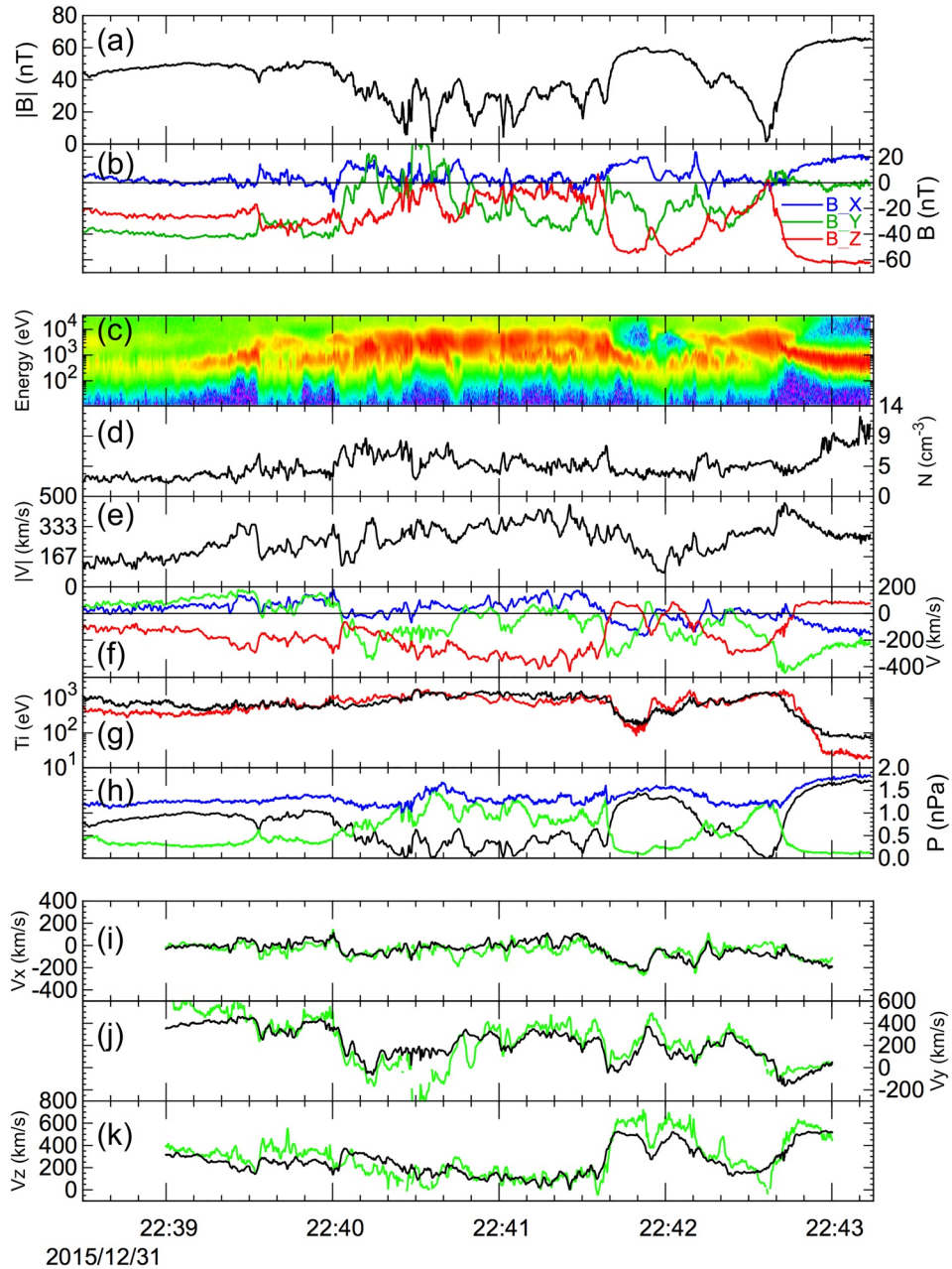

Figure 5. Burst-mode data for the boundary Crossing 2 on December 31, 2015, from the Anomalous Reconnection Layer on the left to the magnetosheath on the right. Panels (a) and (b) show magnitude and Geocentric Solar Ecliptic (GSE) components of the magnetic field. Panel (c) shows ion spectrograms, panel (d) ion density, panels (e) and (f) bulk velocity magnitude and GSE components, panel (g) ion temperatures ($T_\perp$ black, $T_\parallel$ red), and panel (h) pressures (magnetic in black, plasma in green, and total in blue). Panels (i–k) show ion bulk velocity components as seen in the deHoffmann-Teller frame (black), plotted together with corresponding components of $-\vec{V}_A$ (green).

behavior is inconsistent with this boundary being a complete magnetopause crossing with ongoing reconnection, because there would then be inflow into the layer from its two sides and an associated sign reversal of the correlation between field and flow.

2.3.3. Magnetosheath-to-ARL Crossing

Figure 6 shows the next crossing (at time t3), which is in the opposite sense, that is, from the magnetosheath into the ARL, but is otherwise similar. Again there is first a complete crossing, with associat-

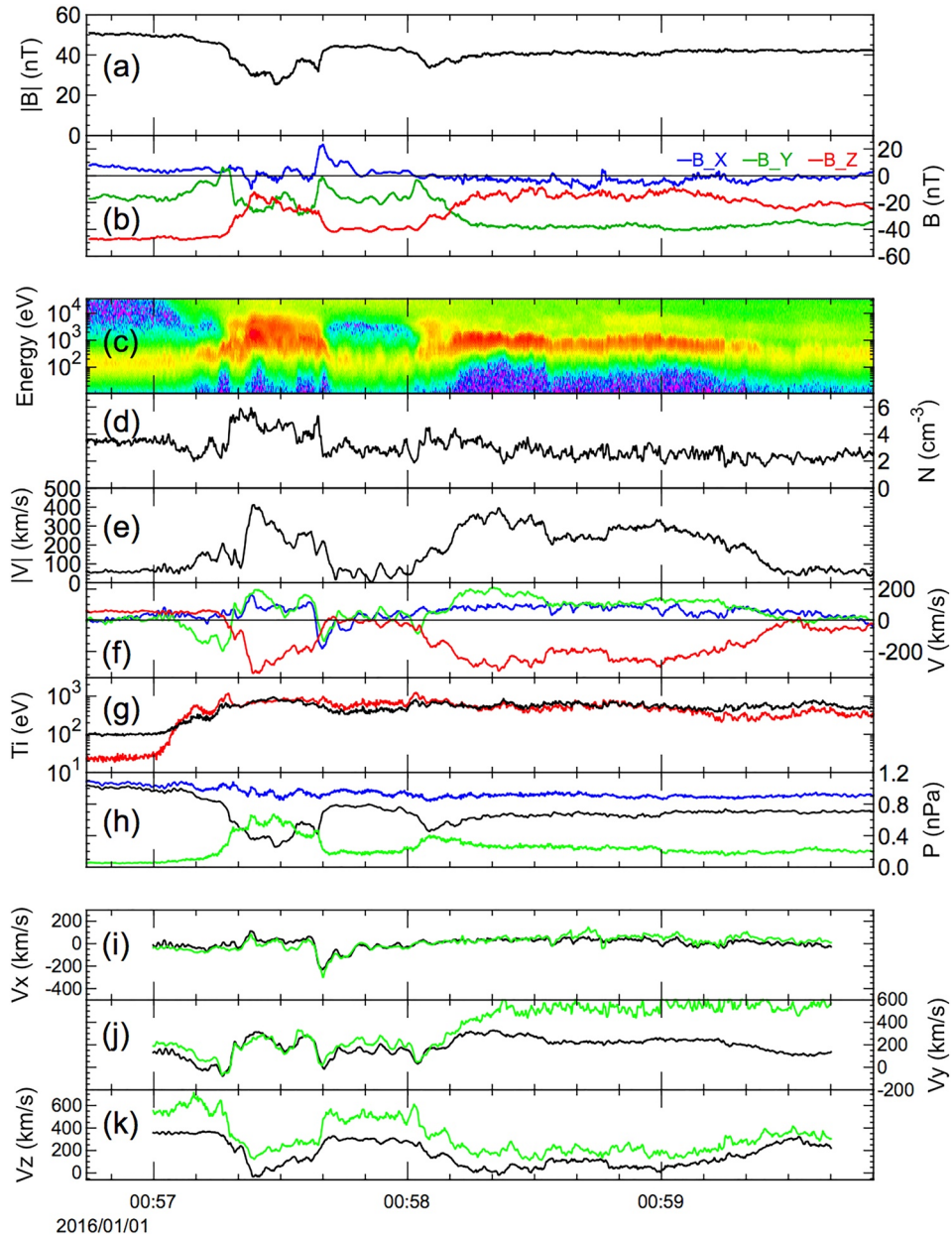

Figure 6. Burst-mode data for the boundary crossing 3 on January 01, 2016 in the same format as Figure 5, but now from the magnetosheath on the left to the Anomalous Reconnection Layer on the right.

ed rise in temperature and ionospheric O^+ density (shown in Figure 3), but then a partial return to the magnetosheath in the interval 00:57 40–00:58 00, before final entry into the ARL. Plasma jetting is also pronounced. The good agreement between $\bar{V}'$ and $-\bar{V}_A$ for the interval up until 00:58:30 UT shown in the bottom frame suggests that this too was an RD crossing, across which magnetosheath plasma flowed into the ARL. In numbers, HTcc = 0.979, Wcc = −0.968, and Wsl = −0.779 for this interval. These results are consistent with those reported by Farrugia et al. (2017) for this crossing. However, even for the full time interval in the figure, there is no sign reversal of the correlation between $\bar{B}$ and $\bar{V}$. This crossing again appears to be an RD with flow from the magnetosheath into the ARL.

While the total pressure varies substantially over the full duration of the interval presented in Figure 3, panel (h) in Figure 6 shows that it is nearly constant during the present boundary crossing, even though the plasma and magnetic field pressures individually show substantial variations.

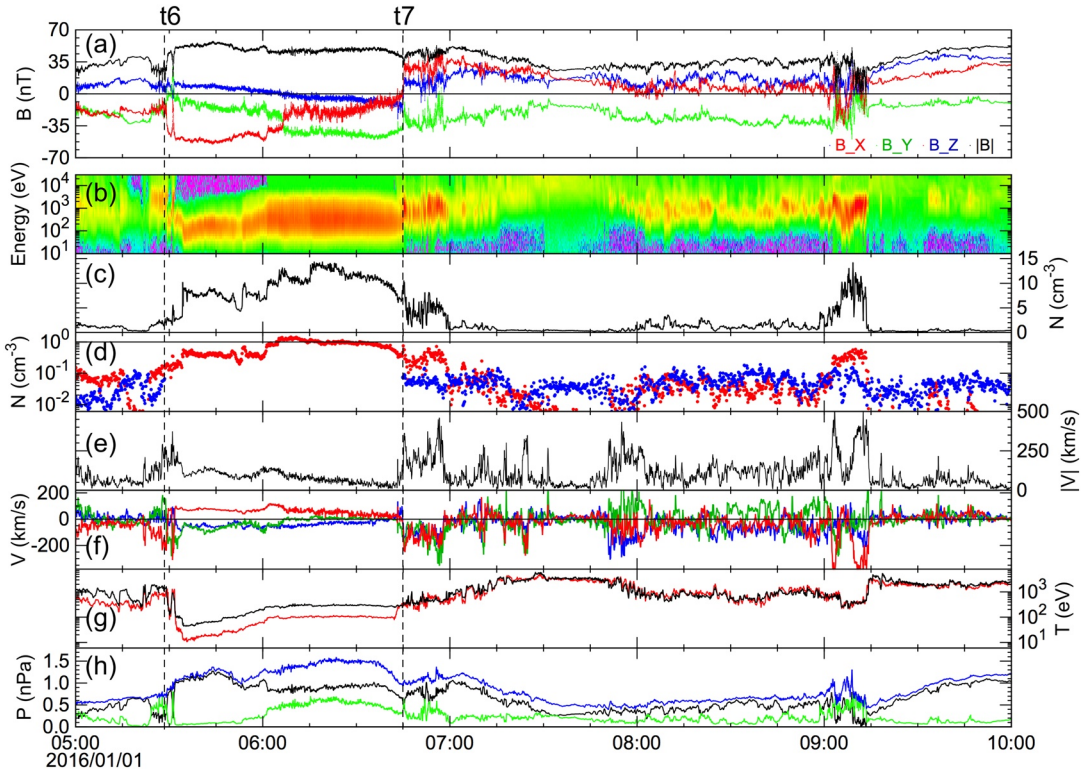

Figure 7. Reentry into the magnetosphere. Format is as in Figure 3, but for the interval 05:00–10:00 UT. No O^+ densities are shown in panel (d) for the interval 05:30–06:45 UT because of "bleed over" from the high H^+ flux.

2.3.4. Reentry Into the Magnetosphere

Figure 7 shows the data for the interval preceding and following the reentry into the magnetosphere, bringing out the following features:

1. The 05:30 transition (labeled t6) from the ARL to the magnetosheath
2. The change in the MMS field at 06:00, caused by a rotation in the IMF (see Figure 2b), accompanied by a temperature increase
3. The start of the inbound crossing of an RD and its associated southward directed jets, at 06:45 (line labeled t7), followed by direct entry into the magnetosphere, without the evidence of an ARL
4. A negative Walén correlation across the RD (see Table A1)
5. A switch to positive Walén correlation (not shown)
6. Exit from this jet at 07:00, followed by a low-density boundary layer until 07:15 UT

This change of sign of the Walén correlation is consistent with the feeding of the southward/dawnward directed magnetopause plasma jet from its two sides, as expected at a location south of a reconnection site.

In the interval 07:15–08:00, the density was extremely low, indicating that MMS had entered the magnetosphere proper, although unexplained velocity spikes also occur. At 08:00, there was a return to the boundary layer. It was followed by a double magnetopause crossing at 09:00, with associated plasma jetting, and then a final entry into the magnetosphere proper at 09:15 UT.

The IMF rotation at 06:00 UT is also evident from the IMF clock angle in panel (h) of Figure 2. That the region from 06:00 to 06:45 is the magnetosheath, and not the ARL, is indicated by the equality of the IMF and MMS 1 clock angles. It is also supported by the elevated total ion density and the high density of He^{++} shown in panels (c) and (d), respectively, of Figure 7. The absence of the ARL at this inbound magnetopause crossing could possibly have been a result of the preceding IMF changes.

Panel (e) in Figure 7 shows that strong plasma jetting occurred at the transition from the ARL to the magnetosheath (near 05:30 UT), at the first inbound magnetopause crossing (at 06:45) and during the brief return to a double magnetopause crossing near 09:00. As the figure shows, the magnetosheath flow velocity dropped to very low values (≈15 km/s) just before the entry into the magnetosphere at 06:45 UT. This behavior is expected from the proximity of MMS at this time to the stagnation point in the subsolar magnetosheath flow.

We note that the rise of the IMF B_z in panel (b) of Figure 2 starts at 05:55 UT, while the rise in the MMS 1 B_z (panel i) occurs more than 10 min later. The propagation delay in the OMNI data is calculated for the subsolar bow shock location rather than the magnetopause location, which can explain at least some of this delay.

2.4. Electron and Ion Pitch Angle Distributions

The pitch angle distributions of electrons and ions can reveal important information about the overall magnetic field configuration.

Figure 8 (top) provides pitch angle information for electrons from the FPI instrument and for energetic protons from EIS. The electron energy spectra in panel (b) show a distinction between the magnetosheath and the ARL. The fluxes in the former region are intense at the lower energies, while in the ARL the fluxes are less intense and occur at higher energy. Some of the transitions between magnetosheath and ARL (at times t2–t6) are seen as brief spikes at higher energies (panel b). Just before the end of the interval shown in the figure, MMS has entered the magnetosphere proper and electrons with energies above 1 keV, typical for the outer magnetosphere, are observed, but they are mostly absent in the ARL (see panel b in Figure 8)

The electron pitch angle distributions in two energy ranges, representing magnetosheath (40–100 eV) and ARL (500–1,000 eV) core populations, are shown in panels (c) and (d). In the ARL intervals (t1–t2, t3–t4, and t5–t6), the 40–100 eV electrons (panel d) have maximum and nearly equal fluxes at 0° and 180°, while the fluxes of 500–1,000 eV electrons (panel c) peak at around 90°. These characteristics are consistent with the ARL being located on closed field lines, with both ends anchored in the ionosphere, implying that reconnection had occurred both north and south of MMS. We note that observations of unidirectional and bidirectional (counter-streaming) electrons have commonly been taken as evidence for open and closed magnetic field lines, respectively (e.g., Fuselier et al., 1997; Hasegawa et al., 2009; Lavraud et al., 2006; McFadden et al., 2008; Mitchell et al., 1987; Øieroset et al., 2015).

If reconnection had only occurred on the northern site, no returning electrons would be observed, except in the special situation where there was a maximum in B somewhere south of MMS, so that electrons with sufficiently large pitch angles would mirror, while electrons with small pitch angles would not. For example, for a field maximum twice the value observed at MMS, the cutoff would be 45°. Such a scenario was reported by Onsager and Scudder (2003) for a boundary layer crossing by the Polar spacecraft, but can be excluded in our case because no dropout at small pitch angles was observed (see Figure 8).

Counterstreaming electrons are, however, not observed throughout the entire ARL. As shown in Figure 9, which is a zoom into an ARL interval, there are patches of unidirectional 0° electrons, implying brief occurrences of open field lines, that is, reconnection occurring only in the north but not in the south. This suggests that the ARL might be a mixture of open and closed field lines. This is in contrast to the magnetosheath intervals (t2–t3, t4–t5, and t6–t7), where the flux intensities at 0° and 180° (especially for 500–1,000 eV electrons) are mostly unbalanced.

At all five boundaries between the ARL and the magnetosheath (at t2, t3, t4, t5, and t6), MMS observed electron signatures of the reconnection separatrix layer. Figure 8 (panels f–k, respectively), shows two such examples. Unidirectional field-aligned heated electrons, with energies up to 10 keV, are seen in the magnetosheath right next to the ARL (panels h and k). This is consistent with the presence of a remote dominant X-line at a northern high-latitude location, producing a separatrix layer outside the reconnection exhaust (e.g., Lavraud et al., 2006; Onsager et al., 2001).

The separatrix layers, especially the one near 00:57 UT in panel (h) of Figure 8 exhibit strong energy dispersion, with the most energetic electrons observed first, that is, extending furthest into the magnetosheath. This is consistent with the remote location of the northern reconnection site.

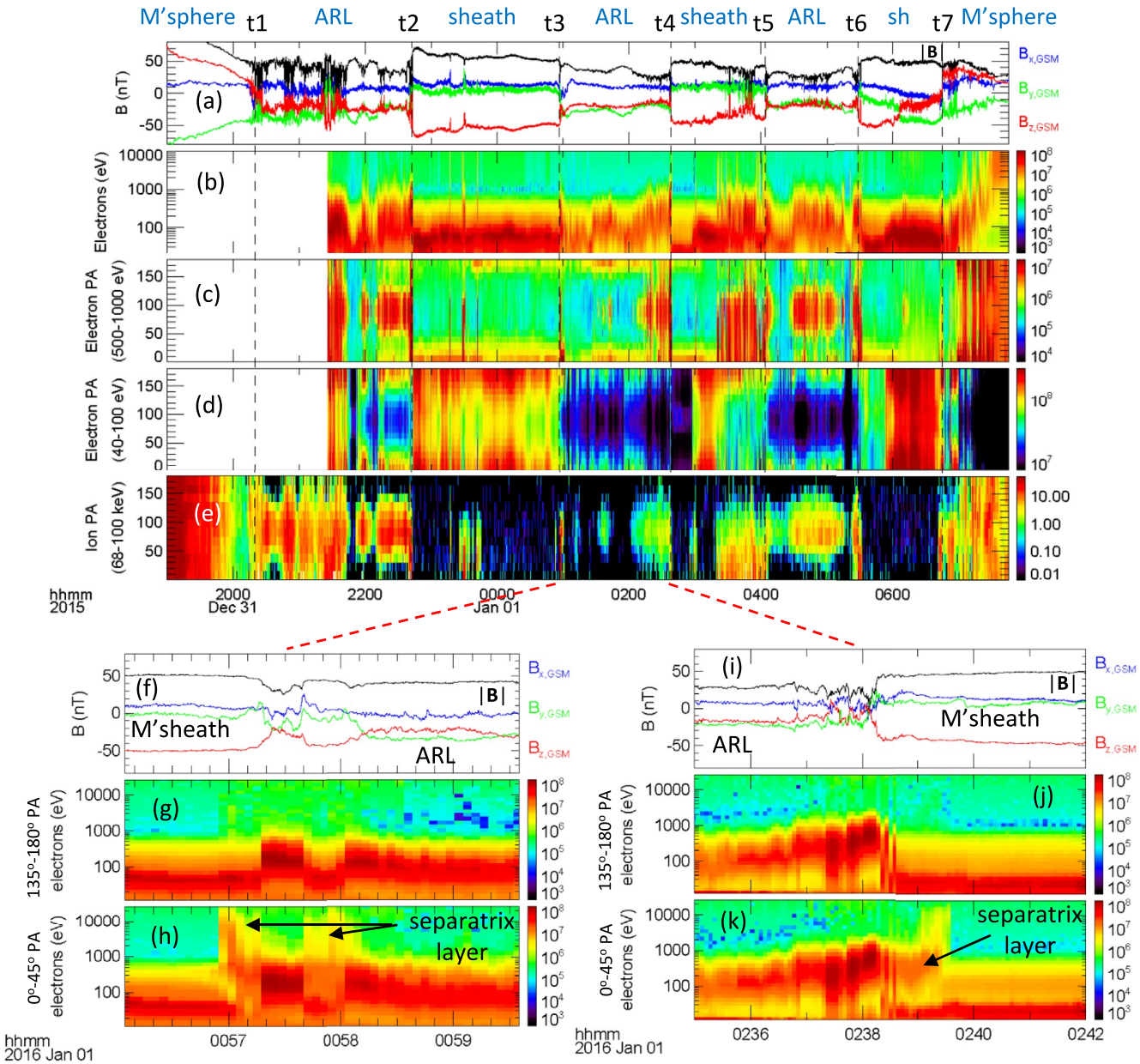

Figure 8. The panels in the top part are (a): magnetic field magnitude and components (from Flux-Gate Magnetometer); (b): energy spectrogram of 20–10,000 eV electrons; (c and d): pitch angle distributions of 500–1,000 and 40–100 eV electrons, respectively (from Fast Plasma Investigation); (e): pitch angle-distribution of energetic (68–100 keV) protons (from Energetic Ion Spectrometer). The electron and ion intensities are given in eV/(cm^2 s sr eV) and counts/s, respectively, coded as shown by the color bars on the right. The bottom plots are expanded views for crossings from the Anomalous Reconnection Layer (ARL) to the magnetosheath and back, respectively. Panels (f) and (i): magnetic field magnitude and components; (g and j): energy spectrograms of electrons at 135°–180° pitch angle, panels (h) and (k): energy spectrograms of electrons at 0°–45° pitch angle.

Panel (e) shows the pitch angle distributions for energetic protons. It indicates the presence in the ARL of trapped particle distributions of magnetospheric origin in a broad angle range around 90°, behavior consistent with particles trapped around a minimum in field strength. In the magnetosheath, the distributions are much weaker and nonsymmetric, indicating a net particle flux in the direction parallel to the magnetic field. At some of the interfaces between magnetosheath and ARL (e.g., at 22:45 and 00:56 UT), there are spikes, narrow in time, of ion flux extending down to 0° pitch angle with no corresponding flux at 180°. This behavior suggests the escape of some ions into the southern magnetosheath along half-open field lines (one "foot" in the ionosphere). Similar MMS observations of escaping ions were reported by Cohen et al. (2016).

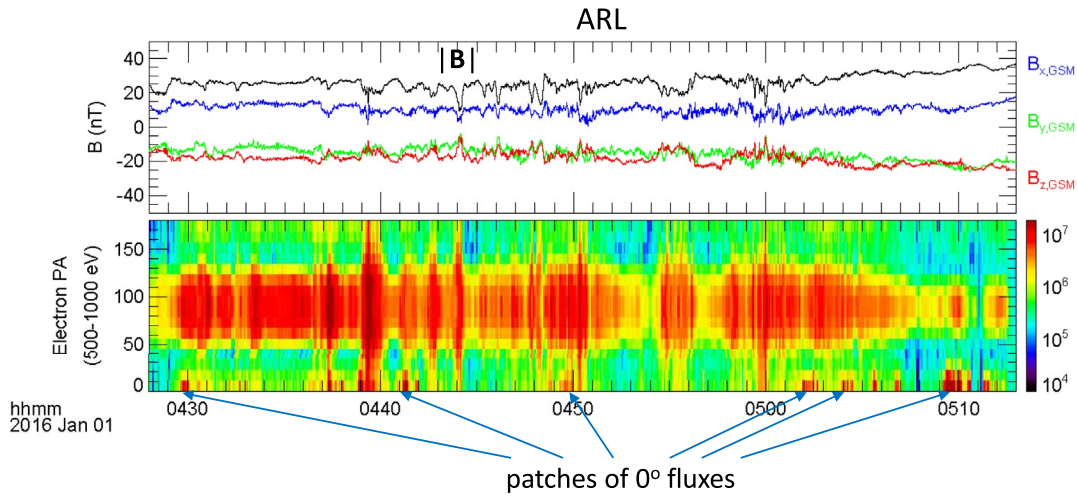

Figure 9. Zoom-in of an Anomalous Reconnection Layer (ARL) showing at the top the magnetic field and at the bottom the pitch angle distributions of 500–1,000 eV electrons. Patches of enhanced 0° electron fluxes, with no equivalent fluxes at 180°, may indicate instances of ARL field lines connected to an *X*-line north of the Magnetospheric Multiscale spacecraft, but un-reconnected (i.e., open) in the southern hemisphere.

3. Summary and Interpretation

3.1. Summary of Observations

The event described in this paper was observed by MMS on December 31, 2015 and on January 1, 2016, on the prenoon side of the magnetosphere and magnetosheath, at low GSE latitudes. It occurred in an approximate GSE longitude range, from −50° during the outward magnetopause crossing to −8° during the inward crossing some 10 h later. A portion of the event has been previously examined by Farrugia et al. (2017). The present paper provides an overview of the total events and a discussion of possible origins of what we refer to as the "Anomalous Reconnection Layer" (ARL). An important aspect of the event is the large dipole tilt during northern hemisphere midwinter, which typically moves magnetopause reconnection sites somewhat northward of the GSE equatorial plane (see, e.g., simulations by Li et al., 2008 and Guo et al., 2020). Observations reported by Hoshi et al. (2018) show that the northward shift is enhanced under lower solar wind Alfvén Mach number conditions. Thus, the present observation of a very broad ARL is a combined effect of low Alfvén Mach number solar wind and large dipole tilt, both of which are rarely satisfied simultaneously.

Strong support that MMS was connected to a reconnection site far north of MMS is provided by the maximum magnetic shear model (Trattner et al., 2007a, 2007b). This empirical model was created by determining the distances to reconnection *X*-lines during hundreds of crossings of the Earth's magnetospheric cusps by the Polar spacecraft. The model has been successfully tested using a wide range of observations. More details of the model and these tests are in a recent review article (Trattner et al., 2021). For the case at hand, that is, stable strongly southward IMF orientation, with B_y small but positive and large dipole tilt, together with the location of MMS on the dawn side, the model (see Figure 10) shows that MMS was likely attached to a high-latitude northern hemisphere reconnection *X*-line that extended from the northern cusp (but lying equatorward of the cusp).

The hour-long ARL intervals were alternated by equally long encounters with the true magnetosheath. They were separated by a current layer, across which the field direction and magnitude changed abruptly, along with changes in plasma density, temperature, temperature anisotropy, pressure, and composition. This current layer contained bursts of southward directed plasma velocities up to 450 km/s. As seen in the HT frame, this flow was approximately Alfvénic, that is, the current layer could be an RD.

As shown in Figure 3, the magnetosheath encounters were characterized by strongly southward magnetic field, consistent with the IMF direction; number of densities ranging from 5 to 15 protons/cm^3; and alpha particles of the order of 4% and, at most, trace amounts of O^+. The plasma flow direction and magnitude

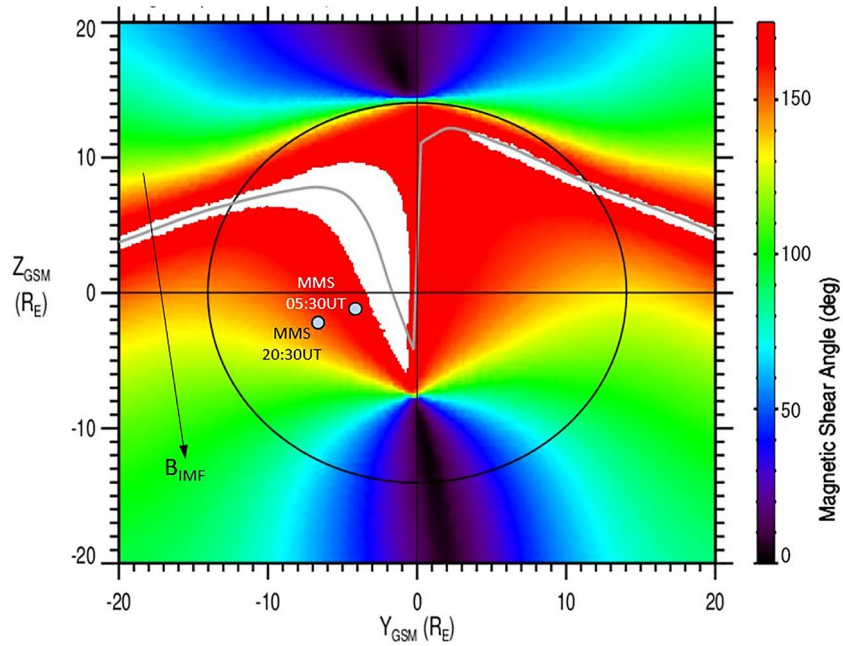

Figure 10. The magnetic shear angle across the dayside magnetopause averaged over the interval from 20:30 to 05:30 UT, with the shear angle coded as shown by the color bar on the right. The view is from the Sun and the shear is projected onto the GSM (Y, Z)-plane, and so is the location of Magnetospheric Multiscale spacecraft at the beginning and end of the time interval. The black arrow labeled B_{IMF} shows the interplanetary magnetic field (IMF) direction averaged over the time interval. The average tilt of the Earth's dipole was −28°. The thin black circular line is the terminator. White regions mark the positions where field lines are antiparallel to within 3°, and the thin gray line is for precisely 180° shear.

were consistent with the MMS location; the temperature anisotropy was typical for the magnetosheath, with $T_\perp > T_{||}$.

In contrast, the ARL was characterized by weaker fields, directed less southward and more dawnward than in the magnetosheath; remarkably low proton number densities (2–3/cm^3); elevated O^+ density levels, and lower, but still significant alpha particle levels; higher temperatures with less anisotropy; lower plasma flow speeds (typically some 50 km/s), directed southward/dawnward; and lower total pressure. The plasma composition makes clear that the entire ARL, along with the magnetopause current layer itself, was, or had been, magnetically connected to the magnetosphere as well as to the magnetosheath.

In all five crossings from the ARL to the magnetosheath and back, a separatrix layer filled with southward streaming heated electrons is observed on the magnetosheath side. The separatrix layer crossings had durations of half a minute or so, while the ARL encounters lasted for more than an hour. This suggests that the long ARL encounters were not the result of some fortuitous match of spacecraft and boundary motion, but that the ARL is much thicker than the separatrix layer, therefore, likely to be very wide (see Figure 11). Inside the ARL electrons are predominantly counterstreaming, consistent with the ARL being mostly on closed field lines.

Interestingly, the magnetosheath flow was persistently northward (see Figure 3, panel f), despite the fact that MMS was located southward of the GSE equatorial plane. This anomalous flow could be due to an MHD (stronger magnetic field) effect, as discussed by Nishino et al. (2008), under southward and weakly sunward IMF conditions that would cause significant northward plasma deflection across the subsolar bow shock under lower Alfvén Mach number solar wind, shifting the stagnation line southward of the Sun-Earth line.

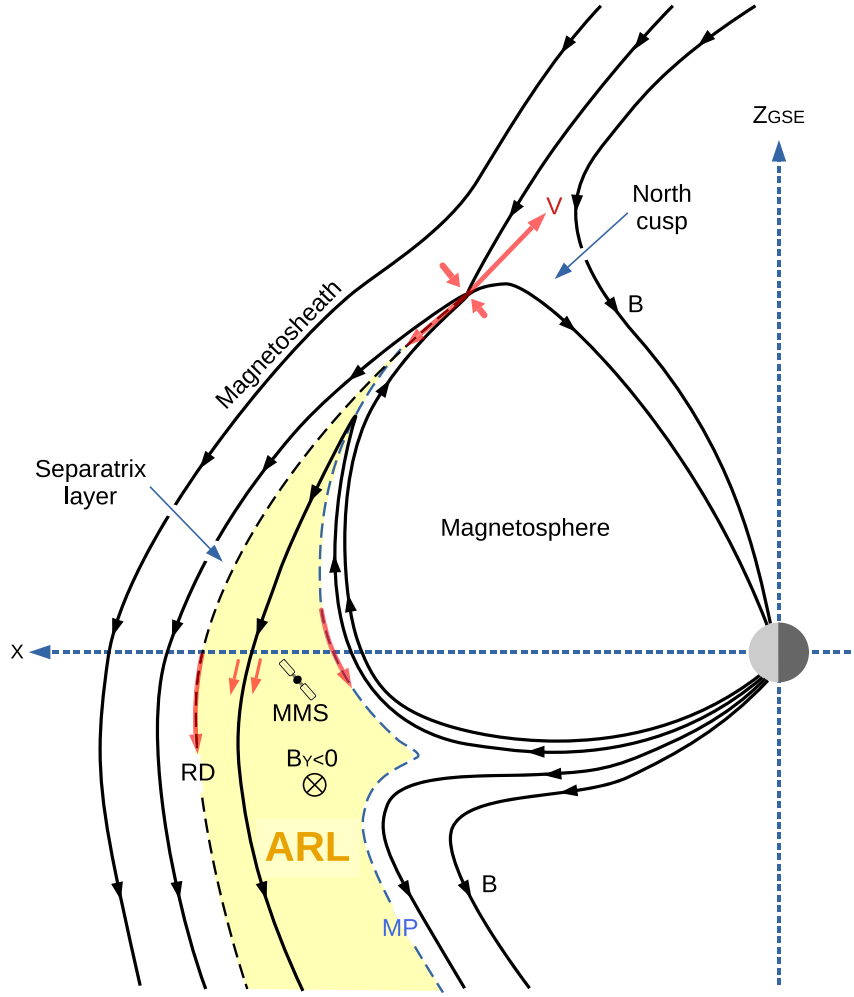

Figure 11. Schematic drawing of a remote reconnection site at high-northern latitudes, leading to the formation of the Anomalous Reconnection Layer (ARL), shown by light yellow shading. Emanating from that reconnection site are a rotational discontinuity (RD), which forms the outer boundary of the ARL, and on its sunward side, a separatrix layer made up of unidirectional flows of heated electrons. Plasma velocities are shown by red arrows. The closed magnetic field topology, inferred from the observed electron pitch angle distributions, implies the existence of a southern reconnection site, whose exact location is not known. MMS, Magnetospheric Multiscale spacecraft.

3.2. Interpretation

Because the observed electron and ion pitch angle distributions suggest that the ARL may have been on closed field lines most of the time, we first explore the possibility that it was part of the magnetosphere itself, as suggested by Farrugia et al. (2017). However, we note that the ARL contained mainly heated magnetosheath ions (with core energy 1 keV), which is not expected in the magnetosphere proper. It is more similar to the cold dense plasma sheet adjacent to the dayside magnetopause previously observed during northward IMF (e.g., Øieroset et al., 2008). Previous models that could account for such a closed-field layer involve the capture of magnetosheath plasmas either by tailward of the cusp reconnection in both hemispheres (Lavraud et al., 2006; Li et al., 2008; Onsager et al., 2001; Raeder et al., 1995; Song & Russell, 1992) or poleward of the cusp reconnection in one hemisphere and tailward of the cusp in the other (Lavraud et al., 2018; Øieroset et al., 2008). All these models are for northward IMF (with or without a strong B_y), which when applied to the present event, would imply that the ARL was formed during the interval of northward/duskward IMF, well before 18:00 UT on December 31.

Two observational facts are inconsistent with the northward IMF formation scenario. First, if the ARL was in reality just an abnormal portion of the outer magnetosphere formed during northward IMF, it would

not have had a negative B_z, given the MMS location well equatorward of the southern cusp throughout the event (see Figure 1). Second, and more important, if reconnection were to occur between field lines in the magnetosheath and those in the ARL, one would expect inflow from both sides into the current layer separating them. But only flow from the magnetosheath, across this RD, into the ARL occurred. This behavior is implied by the anti-field aligned Alfvénic velocities (in the HT frame) and the associated anticorrelation between flow and field seen on both sides. For these reasons, we do not believe that the observed ARL could have been part of the regular magnetosphere with the RD serving as the main magnetopause. Furthermore, a layer of new magnetosphere created during northward IMF (before 18 UT on December 31) is unlikely to survive for 10 h with the presence of magnetopause reconnection during the subsequent southward IMF interval.

The above findings, together with the persistent presence of a separatrix layer, indicative of a dominant *X*-line located far north of the MMS spacecraft, have instead led us to consider the scenario in Figure 11. It shows a schematic, admittedly over-simplified, in which a single reconnection site is located near, but equatorward of the northern cusp. The creation of the ARL is assumed to occur during the southward/sunward turning of the IMF in the interval 18:00–20:00 UT, in the middle of which the large drop in solar wind ram pressure occurred. The resulting increase of Alfvén speed in the solar wind, was further augmented by an increase in an already high-IMF magnitude. As stressed by Farrugia et al. (2017), it even resulted in short intervals of sub-Alfvénic solar wind flow. For the duration of the entire event, sub-Alfvénic magnetosheath flow could have been present near the northern cusp, thus permitting a reconnection site to remain stationary there. Emanating from this site would be a narrow, fast exhaust jet, directed northward/tailward, and a wider, but slower jet, directed equatorward and forming the origin of the ARL. (Note that, when viewed in their respective HT frames, both jets would be Alfvénic.)

A plasma flow component across the RD, from the magnetosheath into the ARL, is an integral part of the scenario. This inflow could have been considerable, as a result of the large Alfvén speeds. The wider, southward-directed jet would have been further widened and therefore further slowed down by the large drop in solar wind ram pressure at 19:00 UT. This pressure drop would have set the RD at the sunward edge of the ARL in an outward motion while having less effect on its earthward edge, which is better anchored to the magnetosphere itself. Note that the southward flow of the plasma in the ARL would decrease significantly as the plasma moves from high latitudes toward the equator. This slowing down is a result of the larger pressure expected near the equator, which is imposed from the magnetosheath through vicinity to the subsolar stagnation point. It provides an explanation for the low velocities seen by MMS in the ARL.

The overall geometry could be compared to that discussed by Levy et al. (1964) for the case of the magnetosphere containing no plasma. In their field configuration, the incoming magnetosheath plasma first encounters an RD in which the tangential field is rotated to agree with that in the magnetosphere, followed slightly later by a slow-mode wave structure, in which the field magnitude adjusts to its value in the magnetosphere and the plasma pressure drops to zero. Usually, the two wave structures are close together and together considered as being the magnetopause. The present event has similarities to this configuration, but with a highly extended temporal separation comprising what we call the ARL between the two standing wave structures. In our model, this separation is the result of the remote location of the reconnection site as well as of the widening caused by the ram pressure drop.

As illustrated by Figure 11, the ARL in this interpretation is on open field lines. This feature appears to be in conflict with the pitch angle information described in Section 2.4, where we had concluded that the ARL was on closed field lines most of the times. A possibility is that the ARL field lines are in reality reconnecting with the magnetospheric field at some location southward of MMS, either equatorward or tailward of the cusp. If it were occurring on the equatorward side, we should have seen northward directed jetting and a separatrix layer with heated electrons at 180° pitch angle, which we do not. Moreover, with both reconnection sites simultaneously active, a flattened magnetic flux rope, draped around the dayside magnetosphere would have been created and then perhaps swept away. The closeness of MMS to the southern cusp, evidenced in Figure 1, might also have had an effect.

If, on the other hand, reconnection were occurring tailward of the southern cusp, that is, further downstream in the geomagnetic tail, then the problem would be the low shear angle between the magnetic fields

between the open field lines of the ARL shown in Figure 11 and the anti-sunward directed magnetospheric field lines. But here, the very low plasma β of ≈0.1 observed in the ARL (see Section 2.2) comes into play. As shown theoretically (Swisdak et al., 2003) and observationally (Phan et al., 2010), reconnection can occur for shear angles as low as 10° provided that β is ≈0.1. These observations pertained to the solar wind, while such low β-values are very rare at the magnetopause (Phan & Paschmann, 1996; Phan et al., 2013). This might explain, together with the extreme dipole tilt, that a structure like the one we report here has not been observed in the past.

As shown in Section 2.4, there is evidence that the field lines in the ARL can be open, albeit only rarely. This would be expected if the reconnection at the northern and the southern sites are not perfectly balanced. For the case of dual lobe reconnection discussed at the beginning of the section, above, the consequences of variable ratios between the reconnection rates at the two sites has been discussed by Lockwood and Moen (1999).

In Section 2.4, it was mentioned that magnetospheric electrons are largely absent in the ARL. To explain the absence, we propose the following scenario: the onset of reconnection at the northern site would cause a quick escape of such electrons along the open field lines into the magnetosheath (e.g., Fuselier et al., 2014). After the field line was closed, any subsequent filling with magnetospheric electrons could be prevented if reconnection at the two sites were usually not occurring simultaneously. This has been proposed by Lavraud et al. (2018) as a reason why magnetospheric electrons are often absent in a similar structure, the low-latitude boundary layer (LLBL).

The LLBL has been reported to be almost always devoid of magnetospheric electrons during both low- and high-shear crossings of the LLBL (Paschmann et al., 1993; Phan & Paschmann, 1996). Even in the case of dayside LLBL crossings during northward IMF that had been reported to be on closed field lines, most do not show magnetospheric electrons (Lavraud et al., 2006). We note that magnetospheric electrons have been observed on closed field lines in several dayside boundary layer cases, created by dual-hemisphere reconnection with northward IMF (Hasegawa et al., 2009; Lavraud et al., 2006, 2018; Øieroset et al., 2008). However, these are rare events (for a different IMF orientation than the present case) that require specific explanations in terms of electron drift and the ordering of reconnection in the two hemispheres.

Furthermore, after the closed ARL is formed, it would convect tailward. At some distance down tail, it is conceivable that magnetospheric electrons could drift onto the old ARL. However, because the MMS observations were on the dayside and the ARL was likely to be continuously formed and convected away, we do not believe there would be enough time for magnetospheric electrons to fully populate the newly created ARL.

In summary, the interpretation presented above accounts for many of the observed ARL features but, even so, it remains partly conjectural. Global numerical simulations using the actually observed, temporally changing, upstream conditions could provide much needed information about the actual mechanism and the plasma entry sites responsible for the creation and features of the ARL, including the observed absence of hot magnetospheric electrons.

Appendix A: Summary of Boundary Crossing Properties

Basic information about the seven boundary crossings is presented in Tables A1 and A2. Table A1 shows the results of the Walén test for the seven boundaries marked in Figure 3, expressed as the Walén regression line slope Walén-slope (Wsl) and correlation coefficient Walén-cc (Wcc). Also given are HTcc, the correlation coefficient for the determination of the deHoffmann-Teller HT frame, in which frame the Walén analysis is performed, and the component of the HT frame velocity along the vector normal to the boundary, which provides a prediction of the boundary velocity, with the ± sign indicating sunward/earthward motion. Details about these calculations are provided in Appendix B. The table shows that the Walén slope is consistently negative, as expected for RD crossings south of a reconnection site. Its magnitude is mostly reasonably close to the ideal value of unity, indicating the approximately Alfvénic flow that characterizes rotational discontinuities (RDs), the only exception being crossing 4.

Table A1
Characteristics of the Crossings

No.	Time (UT)	GSE X, Y, Z (R_E)	Crossing sense	HTcc	Walén-cc	Walén-slope	$\vec{V}_{HT,N}$ (km/s)
1	20151231 20:20	(5.8, −6.9, −0.7)	Msph→ARL	-	-	-	-
2	20151231 22:42	(8.0, −7.1, 0.9)	ARL→Msh	0.971	−0.960	−0.868	−39.9
3	20160101 00:57	(9.6, −6.6, −1.0)	Msh→ARL	0.977	−0.983	−0.790	19.9
4	20160101 02:38	(10.3, −5.0, 1.07)	ARL→Msh	0.973	−0.890	−0.470	−30.0
5	20160101 04:04	(10.7, −5.3, −1.09)	Msh→ARL	0.933	−0.932	−0.897	-7 ± 8
6	20160101 05:29	(10.8, −4.5, −1.09)	ARL→Msh	0.976	−0.833	−0.984	−40
7	20160101 06:45	(10.7, −3.72, −1.06)	Msh→Msph	0.989	−0.898	−0.859	21.6

Note. Columns 1–4 are the number, time, position, and sense of the boundary crossings, while columns 5–7 show the results of the HT analysis; and the last column shows the normal component of the HT velocity, $\vec{V}_{HT,N}$, with the normal $\vec{N}$ obtained from constrained minimum variance analysis (MVAB0). The analysis techniques are described in Appendix B. Time intervals for the analysis are the same as those in Table A2.

The boundary motion is consistent with the sense of the transition, except for crossing 5, for which the calculated normal velocity is too small for its sign (which should be positive) to be reliable. Overall, the table confirms the conclusion that the observations were not of a multilayered structure in the magnetosheath but of transitions of the MMS back and forth across a single moving, RD-like boundary between the magnetopause, and the ARL. The calculated sense of the inbound magnetopause crossing is also consistent with the actual sense of the traversal. For the lack of plasma data during the outbound magnetopause crossing, the normal speed of the boundary could not be estimated, although its long duration suggests it was small.

The inward/outward motion of the boundary between the ARL and the magnetosheath appears to have been caused by variations in the solar wind ram pressure. This behavior can be seen in Figure 2, where decreases in ram pressure coincide with transitions from the magnetosheath proper to the ARL and increases in ram pressure coincide with transitions back into the magnetosheath. As expected, these transitions involve the fast mode: the density and magnetic field increase or decrease together. In Figure 3, the transitions are also accompanied by an imbalance of total pressure across the current layer: the total pressure increases as MMS transits from the ARL into the magnetosheath proper and decreases in reverse transitions. This imbalance appears to have been a temporal rather than a spatial effect.

Another effect expected from the interaction of a fast mode compression wave from the magnetosheath with the RD is a pile up of magnetic field lines and density on its magnetosheath side, as illustrated in Figure 3, shortly after time t2. The reason is as follows. The normal field component of the RD remains

Table A2
Normal Vectors From MVAB0

No.	Time (UT)	Position	$\vec{N}$	evr
1	20:26:25–20:27:10	(5.8, −6.9, −0.7)	(0.799, 0.029, 0.601)	28.9
2	22:41:00–22:43:00	(8.0, −7.1, 0.9)	(0.978, −0.035, 0.206)	16.3
3	00:57:00–00:58:30	(9.6, −6.6, −1.0)	(0.979, −0.141, 0.150)	17.1
4	02:38:00–22:38:20	(10.3, −5.0, 1.07)	(0.957, 0.191, 0.216)	31.8
5	04:04:25–04:45:00	(10.7, −5.3, −1.09)	(0.895, 0.225, 0.385)	43.6
6	05:29:00–05:29:30	(10.8, −4.5, −1.09)	(0.960, 0.097, 0.264)	21.5
7	06:44:50–06:45:40	(10.7, −3.7, −1.06)	(0.861, −0.139, −0.490)	64.7

Note. Columns 1–5 show, the crossing number, the time interval, the Geocentric Solar Ecliptic (GSE) position, the GSE components of the normal vector, $\vec{N}$, and the eigenvalue ratio, evr, both from MVAB0, respectively.

unchanged so that the density increase from the incoming fast mode compression causes a decrease of the normal component of the Alfvén speed. In this way, the impinging fast compression does not just set the RD in motion and make it thinner, it also throttles the plasma flow through it. The result is enhanced fast mode reflection, manifesting itself as a pileup of density and field. Such pileup is in clear evidence immediately after time t2 in Figure 3. More generally, we infer that interaction with fast mode waves can corrupt results from the use of standard, steady-state jump conditions for RDs and slow mode shocks, especially the laws for mass conservation and for balance of normal stresses.

The velocity spikes at the outer edge of the ARL were approximately Alfvénic and most likely associated with brief encounters by MMS with the RD-like layer separating the ARL from the magnetosheath. The Alfvénic behavior of this layer, and the presence of intense, southward-directed beams of energetic particles in it, indicates the presence of ongoing reconnection at a site somewhere north of MMS. The implication is that there was a small amount of plasma flow across the RD structure from the magnetosheath proper, where the entropy is low (low temperature and high density), into the ARL where the entropy is higher (higher temperature and lower density). A further conclusion, based on the negative Walén correlation (in crossings 2–6 in Table A1), is that there would have been a sunward directed, normal magnetic field component in the RD, although this component was too small to be confirmed and therefore is not shown in Figure 11.

Crossings 3 and 4 were identified by Farrugia et al. (2017) as possible passes of MMS through the ion diffusion region associated with a nearby reconnection site. Detailed analysis of these two crossings can be found in their paper, in which our ARL is referred to as the magnetosphere. No explanation is provided for the strange field orientation (negative B_z) in this magnetosphere. The overall Walén slope for crossing 4 is low (−0.47) with relatively poor correlation coefficient (−0.89) but there is no indication that the cause of these results is the reversal of the Walén slope expected in a crossing near a reconnection site. Crossing 3 also showed no indication of such a slope reversal (see Figure 6).

The normal vectors, $\vec{N}$, used to calculate the normal components of $\vec{V}_{HT}$ in Table A1, are given in Table A2. Although they are generally consistent with the interpretation of the ARL as a layer as well as with what is expected at the MMS locations, it is also clear that the boundaries must have had substantial local/temporal deformations. The full outbound magnetopause crossing has a duration of about 12 min but consists of a succession of partial crossings caused by back and forth motion past the MMS as well as by a three-dimensional structure. The prediction of its normal vector is poor, with a very low eigenvalue ratio (evr = 1.5). However, a nearly complete rapid crossing occurred in the short interval listed in the table. It gave a normal vector $\vec{N}$ of high quality (evr = 28.9), with duration and structure (not shown) often seen at the magnetopause. The orientation of $\vec{N}$ for the inbound magnetopause crossing at 06:45 UT is well determined (evr = 64.7) and has a direction consistent with the MMS location near the equatorial side of the southern cusp. Its duration (50 s), its predicted speed (21.6 km/s), and its resulting width (1,080 km) are all consistent with what is usually seen.

Appendix B: Methods for HT Frame, Walén Test, and Normal Vector

The deHoffmann-Teller (HT) transformation velocity, $\vec{V}_{HT}$, was obtained from the usual procedure of minimizing the ion convection electric field in the moving (HT) frame (Khrabrov & Sonnerup, 1998). The correlation coefficient, HTcc, between the components of the computed convection electric field, $\vec{E}_C = -\vec{V} \times \vec{B}$, and the corresponding components of the electric field in the HT frame, $\vec{E}_{HT} = -\vec{V}_{HT} \times \vec{B}$, was then taken as the quality measure of the frame.

For the seven boundaries identified in Figure 3, the HTcc values are given in Table A1. The purpose of the Walén test is to establish how close the plasma velocity, after transformation to the HT frame, was to ± the Alfvén velocity $\vec{V}_A = \vec{B}\sqrt{(1-\alpha)/(\mu_0\rho)}$, with the + sign for parallel flow along $\vec{B}$, as occurs north of a magnetopause reconnection site, and the – sign for antiparallel flow, as occurs south of such a site, as is the case in our event. Good agreement has been frequently used as an indicator of ongoing reconnection at the magnetopause, where an RD should be present to adjust the field direction from that in the magnetosheath to that in the magnetosphere (Levy et al., 1964). As is done in Table A1, the results of the test can be presented as the regression line slope, Wsl, in a scatter plot (not shown) of the velocity components in the HT

frame, that is, the components of $\vec{V}' = \vec{V} - \vec{V}_{HT}$, versus the corresponding components of $\vec{V}_A$ together with the corresponding correlation coefficient Wcc. Alternatively, a visual impression of the level of agreement can be provided by plotting each component of $\vec{V}'$ together with the corresponding component of $\vec{V}_A$, as is illustrated in Figures 5 and 6 (e.g., Paschmann & Sonnerup, 2008).

The vectors $\vec{N}$, normal to the boundaries, were determined by the use of the minimum variance analysis of the magnetic field, constrained by requiring the average field component along $\vec{N}$ to be zero (MVAB0). The method, originally proposed by A. V. Khrabrov, is described by Sonnerup and Scheible (1998). At the magnetopause, where the normal component of $\vec{B}$ is usually small, MVAB0 tends to give more reliable normal directions than the unconstrained MVAB; the price paid is the loss of information about the actual magnitude and sense of the normal magnetic field component.

Data Availability Statement

All MMS data are publicly available through the following URL: https://lasp.colorado.edu/mms/sdc/public/.

Acknowledgments
The AE index is available at the World Data Center for Geomagnetism, Kyoto, Japan. G. Paschmann was supported by a guest status at MPE, Garching. Research efforts by B. U. Ö. Sonnerup were supported by the NASA grant 80NSSC19K0254 to Dartmouth College, those by S. Haaland by the Norwegian Research Council under grant 223252, those by T. Phan by NASA grants NNX17AE12G and 80NSSC18K1380. Research at Southwest Research Institute was funded by the NASA MMS prime contract NNG04EB99C. Open access funding enabled and organized by Projekt DEAL.

References

Cohen, I. J., Mauk, B. H., Anderson, B. J., Westlake, J. H., Sibeck, D. G., Giles, B. L., et al. (2016). Observations of energetic particle escape at the magnetopause: Early results from the MMS Energetic Ion Spectrometer (EIS). *Geophysical Research Letters*, *43*(12), 5960–5968. https://doi.org/10.1002/2016GL068689

Farrugia, C. J., Lugaz, N., Alm, L., Vasquez, B., Argall, M. R., Kucharek, H., et al. (2017). MMS observations of reconnection at dayside magnetopause crossings during transitions of the solar wind to sub-Alfvénic flow. *Journal of Geophysical Research: Space Physics*, *122*(10), 9934–9951. https://doi.org/10.1002/2017JA024563

Fuselier, S. A., Anderson, B. J., & Onsager, T. G. (1997). Electron and ion signatures of field line topology at the low-shear magnetopause. *Journal of Geophysical Research*, *102*(A3), 4847–4863. https://doi.org/10.1029/96JA03635

Fuselier, S. A., Petrinec, S. M., Trattner, K. J., & Lavraud, B. (2014). Magnetic field topology for northward IMF reconnection: Ion observations. *Journal of Geophysical Research: Space Physics*, *119*(11), 9051–9071. https://doi.org/10.1002/2014JA020351

Guo, Z., Lin, Y., Wang, X., Vines, S. K., Lee, S. H., & Chen, Y. (2020). Magnetopause reconnection as influenced by the dipole tilt under southward IMF conditions: Hybrid simulation and MMS observation. *Journal of Geophysical Research: Space Physics*, *125*. https://doi.org/10.1029/2020JA027795

Hasegawa, H., McFadden, J. P., Constantinescu, O. D., Bogdanova, Y. V., Wang, J., Dunlop, M. W., et al. (2009). Boundary layer plasma flows from high-latitude reconnection in the summer hemisphere for northward IMF: THEMIS multi-point observations. *Geophysical Research Letters*, *36*(15), L15107. https://doi.org/10.1029/2009GL039410

Hoshi, Y., Hasegawa, H., Kitamura, N., Saito, Y., & Angelopoulos, V. (2018). Seasonal and solar wind control of the reconnection line location on the Earth's dayside magnetopause. *Journal of Geophysical Research: Space Physics*, *123*(9), 7498–7512. https://doi.org/10.1029/2018JA025305

Kantrowitz, A. R., & Petschek, H. E. (1966). MHD characteristics and shock waves. In W. Kunkel (Ed.), *Plasma physics in theory and application* (p. 148). McGraw-Hill.

Khrabrov, A. V., & Sonnerup, B. U. Ö. (1998). deHoffmann-Teller analysis. In G. Paschmann, & P. W. Daly (Eds.), *Analysis methods for multi-spacecraft data* (p. 221). ESA Publications Division.

Lavraud, B., Jacquey, C., Achilli, T., Fuselier, S. A., Grigorenko, E., Phan, T. D., et al. (2018). Concomitant double ion and electron populations in the Earth's magnetopause boundary layers from double reconnection with lobe and closed field lines. *Journal of Geophysical Research: Space Physics*, *123*(7), 5407–5419. https://doi.org/10.1029/2017JA025152

Lavraud, B., Thomsen, M. F., Lefebvre, B., Schwartz, S. J., Seki, K., Phan, T. D., et al. (2006). Evidence for newly closed magnetosheath field lines at the dayside magnetopause under northward IMF. *Journal of Geophysical Research*, *111*(A5), A05211. https://doi.org/10.1029/2005JA011266

Levy, R. H., Petschek, H. E., & Siscoe, G. L. (1964). Aerodynamic aspects of the magnetospheric flow. *AIAA Journal*, *2*, 2065–2076. https://doi.org/10.2514/3.2745

Li, W., Raeder, J., Thomsen, M. F., & Lavraud, B. (2008). Solar wind plasma entry into the magnetosphere under northward IMF conditions. *Journal of Geophysical Research*, *113*(A4), A04204. https://doi.org/10.1029/2007JA012604

Lockwood, M., & Moen, J. (1999). Reconfiguration and closure of lobe flux by reconnection during northward IMF: Possible evidence for signatures in cusp/cleft auroral emissions. *Annales Geophysicae*, *17*(8), 996–1011. https://doi.org/10.1007/s00585-999-0996-2

Mauk, B. H., Blake, J. B., Baker, D. N., Clemmons, J. H., Reeves, G. D., Spence, H. E., et al. (2016). The energetic particle detector (EPD) investigation and the energetic ion spectrometer (EIS) for the Magnetospheric Multiscale (MMS) mission. *Space Science Reviews*, *199*, 471–514. https://doi.org/10.1007/s11214-014-0055-5

McFadden, J. P., Phan, T. D., Carlson, C. W., Angelopoulos, V., Glassmeier, K. H., & Auster, U. (2008). Structure of the subsolar magnetopause regions during northward IMF: First results from THEMIS. *Geophysical Research Letters*, *35*(17), L17S09. https://doi.org/10.1029/2008GL033630

Mitchell, D. G., Kutchko, F., Williams, D. J., Eastman, T. E., Frank, L. A., & Russell, C. T. (1987). An extended study of the low-latitude boundary layer on the dawn and dusk flanks of the magnetosphere. *Journal of Geophysical Research*, *92*(A7), 7394–7404. https://doi.org/10.1029/JA092iA07p07394

Nishino, M. N., Fujimoto, M., Phan, T.-D., Mukai, T., Saito, Y., Kuznetsova, M. M., & Rastätter, L. (2008). Anomalous flow deflection at Earth's low-Alfvén-Mach-number bow shock. *Physical Review Letters*, *101*(6), 065003. https://doi.org/10.1103/PhysRevLett.101.065003

Øieroset, M., Phan, T. D., Angelopoulos, V., Eastwood, J. P., McFadden, J., Larson, D., et al. (2008). THEMIS multi-spacecraft observations of magnetosheath plasma penetration deep into the dayside low-latitude magnetosphere for northward and strong by IMF. *Geophysical Research Letters*, *35*(17), L17S11. https://doi.org/10.1029/2008GL033661

Øieroset, M., Phan, T. D., Gosling, J. T., Fujimoto, M., & Angelopoulos, V. (2015). Electron and ion edges and the associated topology of the reconnecting magnetopause. *Journal of Geophysical Research: Space Physics*, *120*, 9294–9306. https://doi.org/10.1002/2015JA021580

Onsager, T. G., & Scudder, J. D. (2003). Low-latitude boundary layer formation by magnetic reconnection. *Geophysical Monograph Series*, *133*, 111–120. https://doi.org/10.1029/133GM11

Onsager, T. G., Scudder, J. D., Lockwood, M., & Russell, C. T. (2001). Reconnection at the high-latitude magnetopause during northward interplanetary magnetic field conditions. *Journal of Geophysical Research*, *106*(A11), 25467–25488. https://doi.org/10.1029/2000JA000444

Paschmann, G., Baumjohann, W., Sckopke, N., Phan, T. D., & Luehr, H. (1993). Structure of the dayside magnetopause for low magnetic shear. *Journal of Geophysical Research*, *98*(A8), 13409–13422. https://doi.org/10.1029/93JA00646

Paschmann, G., & Sonnerup, B. U. O. (2008). Proper frame determination and Walen test. *ISSI Scientific Reports Series*, *8*, 65–74.

Phan, T. D., Gosling, J. T., Paschmann, G., Pasma, C., Drake, J. F., Øieroset, M., et al. (2010). The dependence of magnetic reconnection on plasma β and magnetic shear: Evidence from solar wind observations. *Astrophysical Journal Letters*, *719*(2), L199–L203. https://doi.org/10.1088/2041-8205/719/2/L199

Phan, T. D., & Paschmann, G. (1996). Low-latitude dayside magnetopause and boundary layer for high magnetic shear 1. Structure and motion. *Journal of Geophysical Research*, *101*(A4), 7801–7815. https://doi.org/10.1029/95JA03752

Phan, T. D., Paschmann, G., Gosling, J. T., Oieroset, M., Fujimoto, M., Drake, J. F., & Angelopoulos, V. (2013). The dependence of magnetic reconnection on plasma β and magnetic shear: Evidence from magnetopause observations. *Geophysical Research Letters*, *40*(1), 11–16. https://doi.org/10.1029/2012GL054528

Pollock, C., Moore, T., Jacques, A., Burch, J., Gliese, U., Saito, Y., et al. (2016). Fast plasma investigation for Magnetospheric Multiscale. *Space Science Reviews*, *199*, 331–406. https://doi.org/10.1007/s11214-016-0245-4

Raeder, J., Walker, R. J., & Ashour-Abdalla, M. (1995). The structure of the distant geomagnetic tail during long periods of northward IMF. *Geophysical Research Letters*, *22*(4), 349–352. https://doi.org/10.1029/94GL03380

Russell, C. T., Anderson, B. J., Baumjohann, W., Bromund, K. R., Dearborn, D., Fischer, D., et al. (2016). The Magnetospheric Multiscale magnetometers. *Space Science Reviews*, *199*, 189–256. https://doi.org/10.1007/s11214-014-0057-3

Song, P., & Russell, C. T. (1992). Model of the formation of the low-latitude boundary layer for strongly northward interplanetary magnetic field. *Journal of Geophysical Research*, *97*(A2), 1411–1420. https://doi.org/10.1029/91JA02377

Sonnerup, B. U. Ö., & Scheible, M. (1998). Minimum and maximum variance analysis. In G. Paschmann, & P. W. Daly (Eds.), *Analysis methods for multi-spacecraft data* (pp. 185–220). ESA Publications Division.

Swisdak, M., Rogers, B. N., Drake, J. F., & Shay, M. A. (2003). Diamagnetic suppression of component magnetic reconnection at the magnetopause. *Journal of Geophysical Research*, *108*(A5), 1218. https://doi.org/10.1029/2002JA009726

Trattner, K. J., Mulcock, J. S., Petrinec, S. M., & Fuselier, S. A. (2007a). Location of the reconnection line at the magnetopause during southward IMF conditions. *Geophysical Research Letters*, *34*(3), L03108. https://doi.org/10.1029/2006GL028397

Trattner, K. J., Mulcock, J. S., Petrinec, S. M., & Fuselier, S. A. (2007b). Probing the boundary between antiparallel and component reconnection during southward interplanetary magnetic field conditions. *Journal of Geophysical Research*, *112*(A8), A08210. https://doi.org/10.1029/2007JA012270

Trattner, K. J., Petrinec, S. M., & Fuselier, S. A. (2021). The location of magnetic reconnection at Earth's magnetopause. *Space Science Reviews*, *217*(3), 41. https://doi.org/10.1007/s11214-021-00817-8

Young, D. T., Burch, J. L., Gomez, R. G., De Los Santos, A., Miller, G. P., Wilson, P., et al. (2016). Hot plasma composition analyzer for the Magnetospheric Multiscale mission. *Space Science Reviews*, *199*, 407–470. https://doi.org/10.1007/s11214-014-0119-6